Low-temperature time-domain terahertz spectroscopy of terbium gallium garnet crystals

R. V. Mikhaylovskiy,* E. Hendry, F. Y. Ogrin, and V. V. Kruglyak†
School of Physics, University of Exeter, Stocker Road, Exeter EX4 4QL, United Kingdom
(Received 21 November 2012; revised manuscript received 21 February 2013; published 14 March 2013)

We report an experimental observation of high frequency magnetic excitations in terbium gallium garnet crystals using terahertz time-domain spectroscopy. We show that precessional modes of terbium magnetic sublattices can be excited by a magnetic field of a terahertz broadband pulse. We study and discuss the dependence of the observed resonances upon the temperature and the strength and orientation of the bias magnetic field. The behavior of the observed magnetic modes is in agreement with the theory of paramagnetic resonance in the multisublattice system. We also show that the illumination of the crystal with intense optical pulses destroys the magnetic ordering. Our results demonstrate that the time-domain terahertz spectroscopy can be a powerful tool by which to study high frequency properties of dielectric magnetic materials, with perceived extensions to studies in femtomagnetism and magnonics.

DOI: 10.1103/PhysRevB.87.094414 PACS number(s): 76.50.+g, 78.47.D−

I. INTRODUCTION

The time-domain terahertz (THz) spectroscopy has proven to be an effective tool in experimental condensed matter physics.[1] THz radiation is sensitive to a variety of solid state excitations, in particular, including free carriers, polarons, and excitons. The spectra of many important organic molecules, including proteins and DNA, as well as phonon resonances in crystals, lie in the THz region. As an all-optical technique, the THz time-domain spectroscopy is contact free and does not contaminate the samples. The low intensity levels of THz radiation also ensure that the testing is nondestructive.

At present, the THz spectroscopy is routinely used to investigate the electron dynamics in many physical systems (see, e.g. Ref. 2, for a review). However, up to now, only a minor fraction of THz investigations has focused on magnetically ordered systems. Importantly, the frequencies of magnetic resonances of most multisublattice magnetic materials (e.g., rare-earth garnets) lie in the THz frequency range. Thus, the THz time-domain spectroscopy could be potentially useful to investigate magnetic properties of such materials, serving, e.g., as a direct probe of magnetic phase transitions. For example, a successful use of nonlinear THz spectroscopy to study the spin dynamics in NiO was reported in Ref. 3. Some relevant work has been done in the related field of multiferroics, where THz spectroscopy has facilitated the observation of electromagnons.[4] The renaissance of interest in magnetic dielectrics driven by the emerging field of femtomagnetism (see, e.g., Ref. 5 for a review) opens an exciting perspective for application of the technique as an experimental tool that is complementary to more conventional optical pump-probe methods. However, a question still remains as to whether the weak magnetic field of a THz pulse can interact sufficiently strongly with the spin subsystem of a sample, and so, relatively few attempts to implement THz time-domain spectroscopy in the area of magnetism have been undertaken so far. Very recently, an excitation of the quasiferromagnetic mode in $YFeO_3$ by the magnetic field of the terahertz broadband pulse was reported.[6] However, Zhou *et al*. did not perform any studies of the temperature dependence of the observed oscillation and did not apply static magnetic field. So, little information about the magnetic properties of the material was inferred from the measurements.

In this paper, we demonstrate that the time-domain THz spectroscopy can resolve magnetic excitations in terbium gallium garnet (TGG) crystals, thereby proving that THz transients do couple to the spin subsystem in the paramagnetic phase. We study the dependence of the observed magnetic modes upon the bias magnetic field, temperature, and crystal orientation. Finally, we explore a light-induced change in the THz response of the sample.

The measurements were performed on $10 \times 10 \times 1$ mm^3 single crystals of TGG cut along the (111) and (001) planes. TGG is a member of a family of rare-earth garnets that are known for their intricate magnetic structure.[7] TGG has very favorable optical properties for our experimental technique, as it is transparent in both the optical and THz frequency range. At the same time, TGG is widely used in laser technology, e.g., within Faraday rotators, and so its study could be interesting beyond the fundamental point of view.

II. THEORY

TGG is a magnetic material with Ising spin and a Néel temperature of $T_N = 0.35$ K.[8] Thus, at temperatures above T_N it is a paramagnet. Magnetic moments of rare-earth ions in the garnet structure form six different sublattices and a magnetic moment of an ion has its local axes oriented in three orthogonal directions in the triangle, producing a multiaxis magnet with an orientation dependent response.[8,9] For example, the static magnetization and thermal conductivity of TGG measured in a magnetic field demonstrate the anticipated anisotropy.[10,11] Furthermore, this leads to the appearance of six different magnetic resonances instead of one. The modes depend strongly upon the crystal orientation in the bias field **B**, as described below.

The frequency of the paramagnetic resonance ν due to the bias magnetic field **B** is given by Zeeman formula

$$h\nu = g\mu_B B, \tag{1}$$

where g is the Landé factor of an electron and μ_B is the Bohr magneton. However, the simple Zeeman formula is valid for an

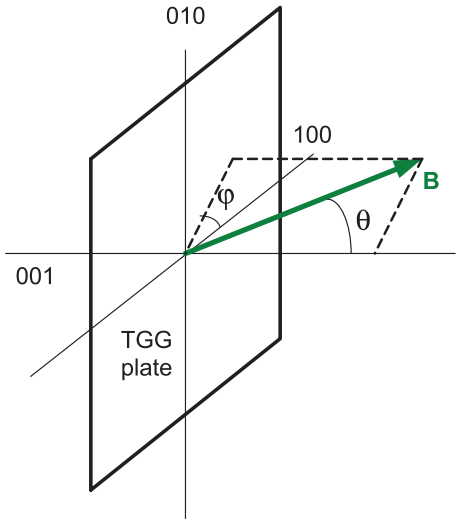

FIG. 1. (Color online) The orientation of the magnetic field with respect to the crystal plate cut along the 001 plane.

isolated atom only. The crystallographic environment greatly changes the magnetic resonance properties of an ion due to crystal field level splitting. Phenomenologically, the impact of the crystal field and spin-orbit coupling can be expressed in terms of the so-called effective g tensor.[12] The principal axes of this tensor are determined by the local fields, i.e., by the local atomic arrangement. In this formalism, one can write the component of the electron Hamiltonian related to the applied magnetic field as

$$H = \mu_B \mathbf{S}\hat{\mathbf{g}}\mathbf{B} = \mu_B S_x g_x B_x + \mu_B S_y g_y B_y + \mu_B S_z g_z B_z, \quad (2)$$

where $\mathbf{S}$ is the electron spin. Here, the axes of the chosen coordinate system coincide with the principal axes of the g tensor. Introducing the effective field $\mathbf{B}' = \frac{1}{2}(g_x B_x \mathbf{i} + g_y B_y \mathbf{j} + g_z B_z \mathbf{k})$ and substituting it to Eq. (2) we arrive at the expression

$$H = 2\mu_B \mathbf{S}\mathbf{B}', \quad (3)$$

which is very similar to the standard Zeeman term. Thus, to calculate the paramagnetic resonance frequency correctly, one needs to substitute $\mathbf{B}'$ instead of $\mathbf{B}$ into Eq. (1). Then, we obtain

$$h\nu = \mu_B \left|\hat{\mathbf{g}}\mathbf{B}\right|. \quad (4)$$

In the case of a multisublattice material, the resonance frequency of the ith sublattice with g tensor $\hat{\mathbf{g}}_i$ is given by

$$h\nu_i = \mu_B \left|\hat{\mathbf{g}}_i \mathbf{B}\right|. \quad (5)$$

The principal axes of g tensors of rare-earth magnetic sublattices in the garnet structure are well known.[9] Thus, projecting the applied magnetic field onto the principal magnetic axes of each sublattice, we can calculate resonance frequencies as a function of the magnetic field orientation according to Eq. (5). In our experiment the magnetic field was oriented along either the 001 or 111 crystallographic direction. Let us consider the case of 001 orientation illustrated in Fig. 1 (the treatment of the 111 orientation is similar, while resulting in bulky formulas). In the measurements, the crystal plate was rotated around both its vertical axis and in plane (i.e., around the normal of the plate). The angle between the magnetic field direction and the sample normal (along the 001 axis in this case) is θ, and the angle between the magnetic field projection onto the sample plane and the 100 axis is φ. In this case, the resonance frequencies are

$$h\nu_1 = \mu_B B\sqrt{g_z^2\cos^2\theta + \tfrac{1}{2}\sin^2\theta\left[g_x^2(1+\sin 2\varphi) + g_y^2(1-\sin 2\varphi)\right]}, \quad (6a)$$

$$h\nu_2 = \mu_B B\sqrt{g_z^2\cos^2\theta + \tfrac{1}{2}\sin^2\theta\left[g_x^2(1-\sin 2\varphi) + g_y^2(1+\sin 2\varphi)\right]}, \quad (6b)$$

$$h\nu_3 = \mu_B B\sqrt{g_z^2\sin^2\theta\cos^2\varphi + \tfrac{1}{2}g_x^2(\sin\theta\sin\varphi+\cos\theta)^2 + \tfrac{1}{2}g_y^2(\sin\theta\sin\varphi-\cos\theta)^2}, \quad (6c)$$

$$h\nu_4 = \mu_B B\sqrt{g_z^2\sin^2\theta\cos^2\varphi + \tfrac{1}{2}g_x^2(\sin\theta\sin\varphi-\cos\theta)^2 + \tfrac{1}{2}g_y^2(\sin\theta\sin\varphi+\cos\theta)^2}, \quad (6d)$$

$$h\nu_5 = \mu_B B\sqrt{g_z^2\sin^2\theta\sin^2\varphi + \tfrac{1}{2}g_x^2(\sin\theta\cos\varphi+\cos\theta)^2 + \tfrac{1}{2}g_y^2(\sin\theta\cos\varphi-\cos\theta)^2}, \quad (6e)$$

$$h\nu_6 = \mu_B B\sqrt{g_z^2\sin^2\theta\sin^2\varphi + \tfrac{1}{2}g_x^2(\sin\theta\cos\varphi-\cos\theta)^2 + \tfrac{1}{2}g_y^2(\sin\theta\cos\varphi+\cos\theta)^2}. \quad (6f)$$

Equations (6) are used below to fit the experimental data.

III. EXPERIMENT

The basic idea of the transmission time-domain THz spectroscopy can be described in the following way. A subpicosecond pulse of electromagnetic radiation passes through the sample. As a result, the temporal profile of the pulse is modified as compared to that of the reference pulse. The latter can be either a freely propagating pulse or a pulse transmitted through a medium with known properties. By analyzing absorption peaks in the normalized Fourier spectra of the pulses transmitted through the sample, one can obtain information about the spectrum of THz excitations in the sample. Furthermore, illuminating the sample by the optical pulse synchronized with the THz pulse, one is also able to study photoinduced dynamics at THz frequencies.

The experimental setup is schematically shown in Fig. 2. The THz spectrometer is powered by a Ti:sapphire laser that emits a train of optical pulses of 800 nm wavelength and a

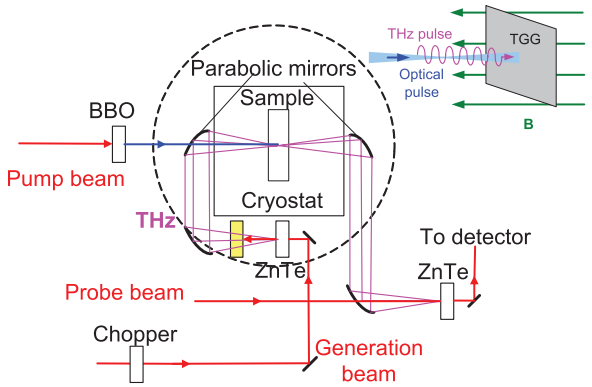

FIG. 2. (Color online) The schematic of the THz spectrometer. The inset illustrates the position of the sample relative to the THz and optical beams and the bias magnetic field.

duration of ∼100 fs at a repetition rate of 1050 Hz. Each pulse is split into a stronger pump and generation pulses and a weaker probe pulse. The generation laser beam is incident onto a ZnTe crystal. The crystal emits THz waves (magenta) that are focused to a TGG sample inside the cryostat with the help of a pair of parabolic mirrors. The second pair of parabolic mirrors collects the transmitted THz pulse and focuses it onto a detection ZnTe crystal to which the probe laser pulse is directed. The standard electro-optical sampling method is then used to record the THz electric field. The pump laser beam goes through the doubling beta barium borate (BBO) crystal and illuminates the sample. The TGG crystal is mounted inside a helium bath cryostat with a 7 T superconducting magnet. The magnet axis is oriented along the THz pulse propagation direction (see in the set in Fig. 2).

In the optically pumped measurements, the intense pump pulse goes through a doubling BBO crystal and is transformed to the second harmonic 400 nm pulse. The remnant 800 nm pulse is filtered out, and the 400 nm pulse illuminates the sample exactly within the area of the THz spot. The diameter of the pump spot on the sample surface is about 1 mm, and the peak intensity is about 10 GW/cm^2.

To record the THz signal, we use a standard electro-optical sampling technique based on the Pockels effect in electro-optical crystals.[13,14] The working frequency range of the spectrometer used in the experiment lies between 100 GHz and 1 THz (see the Appendix). The upper limit is due to the absorption in the cryostat's windows.

IV. RESULTS AND DISCUSSION

To analyze the coupling of excitations to the THz transients, one should convert the measured time resolved signals into the frequency domain. Applying the time Fourier transformation to the time resolved THz wave forms, we arrive to the normalized loss function $\sigma(\nu)$ defined as

$$\sigma(\nu) = -\ln\left(\left|\frac{T(\nu)}{T_{\text{ref}}(\nu)}\right|\right), \tag{7}$$

where $T(\nu)$ is the spectrum of the THz signal transmitted through the sample and $T_{\text{ref}}(\nu)$ is the spectrum of the reference signal. This quantity includes components due to both reflective and absorptive losses.

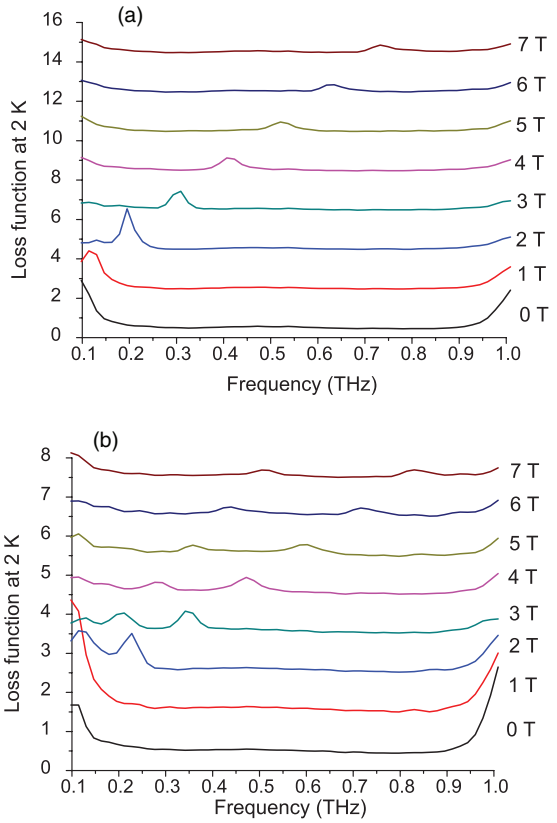

FIG. 3. (Color online) The loss function for different values of bias magnetic field at 2 K in the case of the crystal plate cut along ⟨001⟩ plane. (a) The static magnetic field is applied along the crystal normal (001 axis) exactly. (b) The field is applied with deviation of 11.25° with respect to the crystal normal.

We demonstrate below the evidence for the high frequency magnetic excitations in the range of temperatures between 2 and 15 K. In contrast to the static neutron scattering measurement reported in Ref. 8, the THz spectroscopy allows us to study the dynamical properties of TGG in the high bias magnetic field. The only other techniques that could deliver this kind of information in principle are the inelastic neutron scattering[15] and THz electron spin resonance.[16]

Figure 3 shows THz absorption spectra acquired from the crystal cut along the (001) plane at a temperature of 2 K and different values of the applied magnetic field. A similar pattern is also reproduced at higher temperatures and for the (111) crystal. The curves were obtained using the procedure explained above. In this way, the Fourier amplitudes calculated from the THz signals were normalized by the reference spectrum according to Eq. (1). Then, we extracted the resonance frequencies and amplitudes by fitting the corresponding absorption peaks to Lorentzian curves.

The spectra shown in Figs. 3(a) and 3(b) reveal three resonances. One of the resonances manifests itself as a rising slope at frequencies just below 1 THz, with the resonance frequency lying outside the bandwidth of our spectrometer (see the Appendix). The resonance is most profound at zero bias magnetic field, at which it becomes noticeable below 50 K temperature. As the bias field increases, the peak moves completely outside our measurement window. The resonance

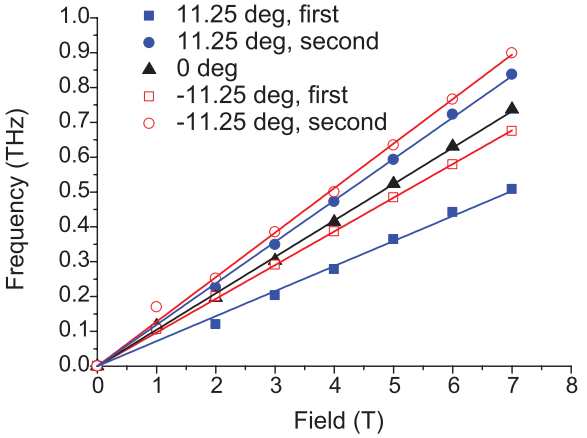

FIG. 4. (Color online) The field dependences of the frequencies of the two low frequency modes are shown for three orientations of the ⟨001⟩ crystal with respect to the bias field.

might well result from the electronic transition at 34 cm^{-1} (1.13 THz) observed in Raman spectra of TGG.[17]

Two other absorption peaks of much lower frequency are generally observed at finite values of the bias magnetic field. Again, the frequencies of the resonances increase as the bias field increases, as can be clearly observed from Fig. 3(b). Importantly, the two peaks merge into one when the bias field is aligned precisely along the 001 axis [Fig. 3(a)]. The behavior suggests that the oscillations responsible for the observed absorption peaks are of magnetic origin. In Fig. 4, the resonance frequencies of the modes, for a fixed temperature, are plotted as a function of the bias magnetic field for three orientations of the bias magnetic field. The graphs display a linear dependence of the resonance frequencies upon the applied magnetic field. The highest frequency mode nearly reaches 1 THz at the field of 7 T. The fact that the observed magnetic absorption lines depend drastically upon the crystal orientation in the bias field reveals anisotropy inherent to the magnetic system and thereby confirms that the g factor associated with the Tb magnetic moments in TGG is a tensor. The two lower frequency magnetic resonances attest the presence of at least two magnetic sublattices. Below, we will focus our attention on the latter two modes, which are more clearly resolved and are definitely magnetic in nature.

The resonance frequencies are shown in Fig. 5(a) as a function of the temperature for three values of the bias magnetic field. Figure 5(b) also shows the temperature dependence of the frequency deviation of the resonances from their frequency value at 2 K. The overlap between the absorption peak of the second magnetic mode at 7 T with the slope of the nonmagnetic mode resulted in the relatively large errors seen in Fig. 5(a). In the Fig. 5(b) these three points are omitted for clarity. A small rise in frequency of both modes (less than 8%) can be observed as the temperature increases. Figure 6 shows the temperature dependence of the resonance peak amplitudes for the field values of 3 and 5 T. As the temperature increases, the amplitudes decrease and fall below the noise level of our experiment above 10 K. We attribute this behavior to the expected hyperbolic decrease of the magnetic susceptibility as the temperature increases, in accord with the Curie-Weiss law.

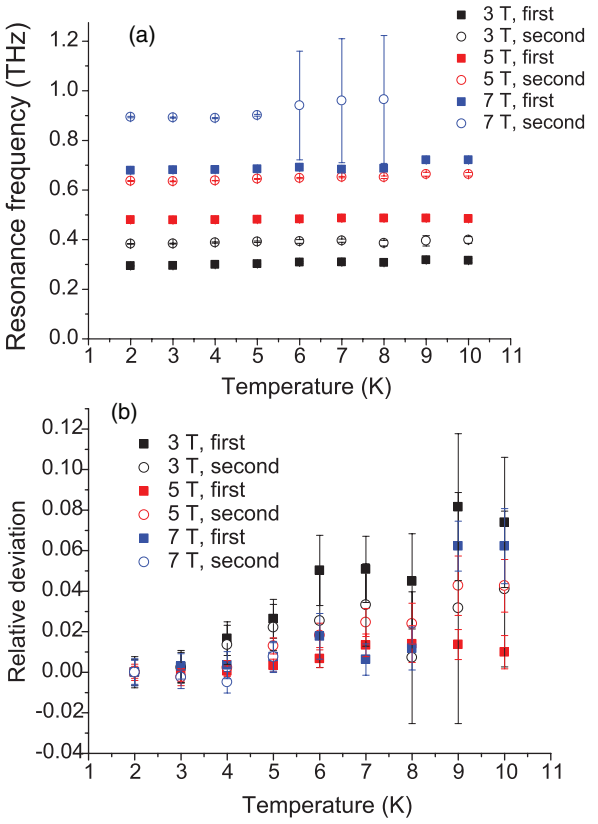

FIG. 5. (Color online) The temperature dependence of the resonance frequencies (a) and their relative deviations from the resonance frequencies at 2 K (b) are shown.

By rotating the sample around its vertical in-plane axis (which corresponds to the direction of the THz magnetic field), we were able to study the dependence of the measured signal upon the orientation of the bias magnetic field relative to the crystal's normal, i.e., the angle θ as defined above. In a separate set of measurements, we rotated the crystals in their planes, so as to investigate any effect of the orientation of the crystallographic axes with respect to the THz pulse polarization. The exemplary dependences of the resonant frequencies of the two magnetic modes are shown in Fig. 7(a)

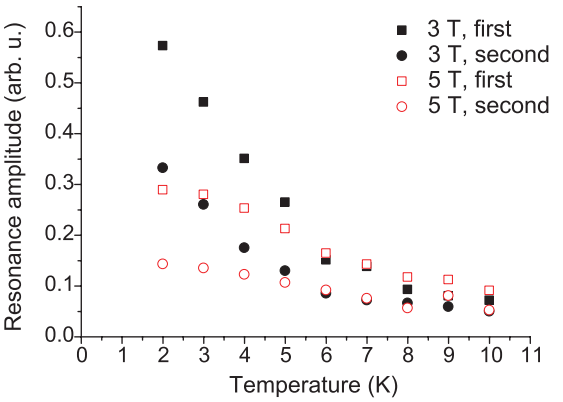

FIG. 6. (Color online) The temperature dependence of the resonance amplitudes.

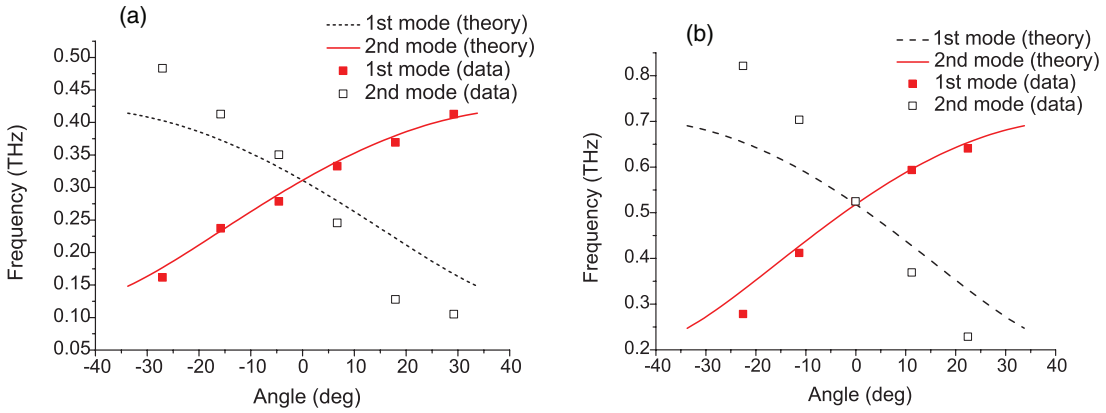

FIG. 7. (Color online) The frequencies of the magnetic resonances in 001 crystal as functions of angle between the magnetic field and the sample normal in the bias fields of (a) 3 T and (b) 5 T. Experimental data are shown together with theoretical curves.

for a 3 T bias field and in Fig. 7(b) for a 5 T bias field in the case when the 010 crystal axis coincides with the direction of the axis of rotation (i.e., with the THz magnetic field). One can clearly see from the figure that the resonance modes converge as the direction of the bias magnetic field approaches the normal to the sample's plane. The experimental data are fitted using Eqs. (6) for a given orientation assuming that the components of the g tensor are $g_x = 3$, $g_y = 10$, $g_z = 12$. These values provide the best agreement between the experimental data and theory in all cases measured in our experiment. Also, we observe, as expected, that the reversal of the applied magnetic field direction does not affect the observed response.

The experimental points depicted in Fig. 7 agree reasonably well with the theoretical model. Yet, some deviation is observed. While the theory predicts symmetric dependences, the experimental results are asymmetric. Moreover, the theory predicts four distinct paramagnetic modes in the case of the 001 crystal orientation that is shown in Fig. 8, while just two modes are observed in the measurements. The calculated curves resemble greatly the analogous dependences characteristic for other rare-earth garnets.[18,19]

One should note that Eqs. (6) do not describe the coupling of the magnetic modes to the ac magnetic field. To explain our experimental data, one needs to analyze the problem of interaction of the magnetic moments of sublattices with the terahertz magnetic field. The development of a rigorous mathematical theory of magnetic dynamics of multisublattice magnets is far from trivial and is beyond the scope of this work. At the same time, one can apply simple geometrical arguments to explain the experimental data. We illustrate this for the situation considered more closely above, i.e., for the 001 crystal plane in the THz field $\mathbf{b}_{\mathrm{THz}}$ aligned along the 100 axis. The orientations of the sublattices' spins are shown in Fig. 9. The net magnetization (i.e., the sum of the magnetizations of all sublattices) is oriented along the bias field as required for a paramagnet. Then one can see that the magnetizations $\mathbf{M}_1$,$\mathbf{M}_2$ and $\mathbf{M}_3$,$\mathbf{M}_4$ pairwise have identical orientations with respect to the bias magnetic field, and so, the corresponding modes are degenerate, which is in accordance with curves shown in Fig. 7. These modes are not observed in the experiment. Indeed, the torque exerted onto ith magnetization is $\sim[\mathbf{M}_i \times \hat{\mathbf{g}}_i \mathbf{b}_{\mathrm{THz}}]$, i.e., the g tensor determines how a specific sublattice reacts to the THz

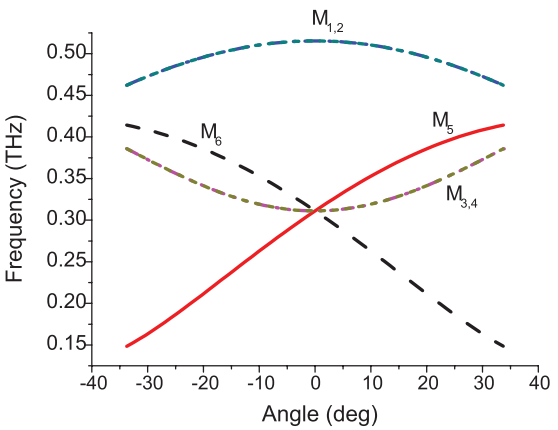

FIG. 8. (Color online) The angular dependences of all degenerate magnetic modes calculated for $\varphi = 0$. The solid and dashed curves are the same as in Fig. 7.

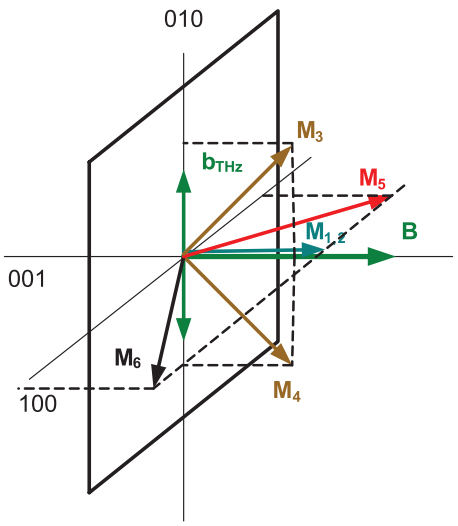

FIG. 9. (Color online) The magnetic structure of the TGG crystal plate cut perpendicular to 001 axis. The bias magnetic field is applied along the 001 axis while the time varying THz field is aligned along the 010 direction. The colors used to depict different sublattices are in correspondence with Fig. 8.

magnetic field. For the particular values of the g-tensor components extracted from the experimental data, it can be shown that the torque exerted on $\mathbf{M}_5$ and $\mathbf{M}_6$ is much larger compared to the torque exerted on the $\mathbf{M}_1$,$\mathbf{M}_2$ and $\mathbf{M}_3$,$\mathbf{M}_4$. This explains why only two modes appear in the absorption spectrum.

One should note that Eqs. (6) are derived under the assumption that the magnetic sublattices do not interact. At the same time, it has been known for decades that rare-earth garnets exhibit magnetic ordering well above their Néel temperatures, provided that a high enough magnetic field is applied.[20] Recently, such a field-induced antiferromagnetic state was also reported for TGG.[8] Kamazawa *et al*. argued that the applied magnetic field breaks the symmetry and thereby enables the metamagnetic phase transition to an antiferromagnetic state. If the antiferromagnetic ordering indeed occurs in our case, then it might be the reason for the frequency asymmetry observed in Fig. 7. However, we did not find any more direct evidence for the metamagnetic phase transition in the present study.

Finally, we explore the effect of optical excitation on the observed THz response. Indeed, if we could modify the magnetic system in TGG through an optical excitation with a femtosecond pulse, we could learn important information about magnetic relaxation dynamics and mechanisms. It is known from all-optical pump-probe experiments that one could expect optically induced effects of thermal or nonthermal origin.[5] In thermal effects, such as laser-induced demagnetization,[21,22] the changes in the magnetic state result from optical absorption followed by a rapid increase of temperature. Nonthermal effects are based on Raman-type nonlinear optical processes, in particular, on the inverse Faraday effect—the generation of nonlinear magnetization by circularly polarized light and/or excitation of the precessional magnetic modes. In both cases, the optical modification of the magnetic state could be expected to manifest itself also in the THz response. The distinctive feature of the nonthermal effects is the sensitivity to the pump light polarization while the thermal optical manipulation is determined by the pump intensity only.

Our setup allows us to pump the sample at two wavelengths, 800 and 400 nm. TGG has an absorption band at 390 nm and is transparent at 800 nm.[23] Also, the Verdet constant, which is commonly assumed to determine the strength of nonthermal optomagnetic effects,[24] is greater at 400 nm than at 800 nm.[23] Thus, one could anticipate that the 400 nm light suits more the goal to modify the magnetic state of TGG.

Indeed, we found that the 800 nm pump light does not affect the THz response of the TGG. At the same time, the THz response of the sample changes significantly as a result of illumination by the 400 nm pump. The photoinduced effect was found to be independent of the time delay between THz and optical pulses. So, we conclude that the light-induced perturbation is extremely long lived, i.e., each femtosecond laser pulse produces an excited state that does not relax within 1 ms (the time interval between the subsequent laser pulses). The loss functions with and without photoexcitation are shown in Fig. 10. One can see that the illumination of the sample ruins the magnetic order since the magnetic absorption peaks disappear completely. The optical pump also induces quite noticeable THz absorption for frequencies lying above

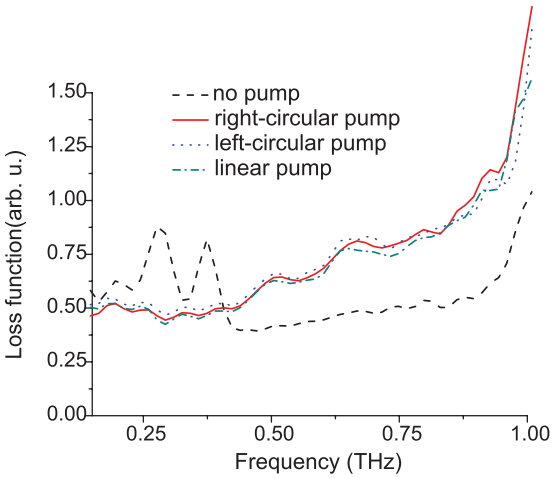

FIG. 10. (Color online) THz absorption peaks in the (111) crystal in the bias magnetic field of 3 at the temperature of 2 K. The dashed curve corresponds to the absence of the optical stimulus. The solid and dotted curves correspond to the circularly polarized pump of opposite helicities while the dashed-dotted line depicts the THz response under the linear polarized pump light.

600 GHz. The effect does not depend on the pump polarization, which rules out any optomagnetic phenomena, such as the inverse Faraday effect.

Based on the previous discussion, it is more likely that the effect has a thermal-like origin. However, it could not be a simple steady heating effect since the additional high frequency absorption is introduced by the optical pumping. This absorption is not observed in the THz responses at any temperature. Hence, we suppose that the 400 nm light excites electronic transitions corresponding to an absorption band in TGG at 390 nm,[23] which subsequently modifies the state of the Tb ions. In addition, subsequent heat transfer to the crystal lattice may also be responsible for the demagnetization effect. The process of the destruction of the magnetic state can be called light-induced demagnetization, which is in this sense similar to the ultrafast demagnetization observed in metallic ferromagnetic films. However, the magnetic state does not recover within 1 ms, in contrast to the previous experiments. Indeed, it is well known that the origin of the magnetic moment in TGG is quite different from the itinerant ferromagnetism of metals such as nickel, iron, and cobalt. The magnetic moment of TGG originates from the Tb ions. The time scale of the relaxation processes of the ions may be quite long compared to the typical times of the free electron dynamics in the ferromagnetic metallic films.

We have also tried to study the THz response of yttrium iron garnet (YIG) and gadolinium gallium garnet (GGG) in the same way (not shown). Surprisingly, YIG does not exhibit resonances within the frequency range of interest. On the other hand, GGG did show magnetic resonances at liquid helium temperatures but with a relatively low frequency of the order of 100 GHz, i.e., exactly on the edge of our working range. We did not observe any interesting features of the mode in GGG. This further supports our interpretation of the signal since it is known that GGG has isotropic g factor of about 2.

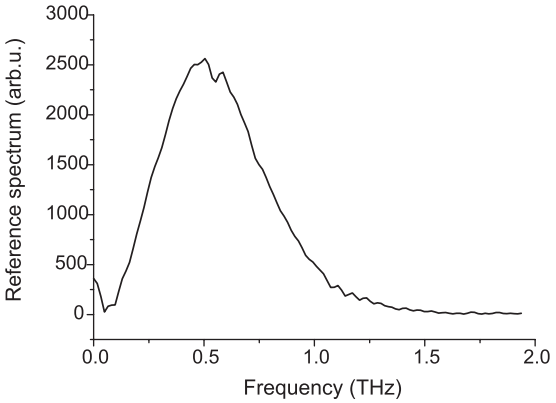

FIG. 11. The reference spectrum.

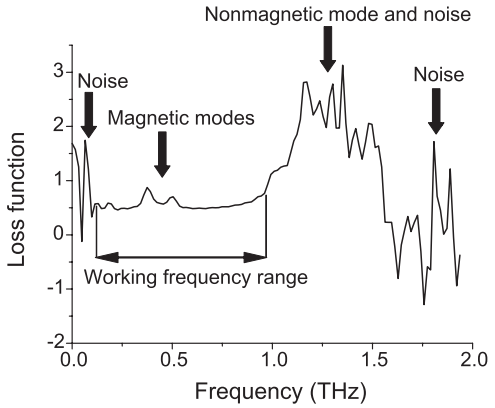

FIG. 12. An example of the loss function experimentally determined from the TGG crystal is shown over the frequency range of 2 THz for the magnetic field of 4 T and the temperature of 2 K.

V. CONCLUSION AND OUTLOOK

To summarize, we have used time-domain THz spectroscopy to study THz magnetic excitations in TGG crystals. We have observed two high frequency (up to 1 THz) precessional modes. We have studied the dependence of the modes on the temperature and the strength and orientation of the bias magnetic field for two TGG crystals cut along the (111) and (001) crystallographic planes. In contrast to the usual paramagnetic resonance, the magnetic excitations demonstrate nontrivial anisotropy, confirming the presence of multiple magnetic sublattices at low temperatures. The observed behavior has been interpreted using a simple model of paramagnetic resonances in the multisublattice system. By comparing the model and experiment, we have been able to extract values of g-tensor components of Tb spins in TGG.

Furthermore, we have shown that intense femtosecond pulses of 400 nm wavelength are able to excite electronic transitions corresponding to the TGG absorption band at 390 nm, which can subsequently modify the magnetic state of Tb ions. Despite the fact that the intense optical pulses change the THz transmission through the sample, the photoexcited state does not relax during a 1 ms time delay between the subsequent laser pulses, demonstrating that the photoexcitation is long lived. Thus, only a steady excited state is built up due to the repeated action of the pulse train. The optical excitation removes the magnetic resonances from the transmission spectra.

We have shown that THz spectroscopy can reveal information about the intricate magnetic structure of Ising spin materials such as TGG, through their high frequency magnetic oscillations. There is an excellent prospect for application of the THz spectroscopy to further magnetic dielectric materials with magnetic resonances in the THz domain. Our findings also have an immense importance for the realization of perceived ultrahigh speed spin wave logic devices and for testing of magnonic metamaterials within the concept of magnonics.[25] The detection of the transient loss of magnetic order suggests that the time-domain THz spectroscopy might also prove to be an important measurement technique by which to study femtomagnetic phenomena.[5] However, the observed long relaxation time of the optically excited state must be taken into account in the design of future THz pump-probe experiments on magnetic dielectrics.

ACKNOWLEDGMENTS

The authors thank S. Hornett, E. Stone, and Y. Au for technical assistance. The research leading to these results has received funding from the European Commission's 7th Framework Programme (FP7/2007-2013) under Grant Agreement No. 228673 (MAGNONICS) and from EPSRC of the UK under Project No. EP/E055087/1.

APPENDIX

The spectrum of THz broadband emission produced via optical rectification of 100 fs laser pulses in ZnTe crystal typically ranges from 100 GHz to 2 THz.[2] However, the quartz windows of our cryostat absorb THz radiation at frequencies above ∼1 THz. The spectrum of the resulting reference THz pulse transmitted through the cryostat is shown in Fig. 11. The signal-to-noise ratio also drops rapidly above 1 THz, as observed from Fig. 12, in which an example of the experimentally determined loss function is shown over the frequency range up to 2 THz. Nonetheless, the presence of the absorption peak above 1 THz is still evident, even though its exact position is beyond the resolution of our spectrometer.

*Corresponding address: rm350@exeter.ac.uk
†Corresponding address: v.v.kruglyak@exeter.ac.uk

[1] M. Hangyo, M. Tani, and T. Nagashima, Int. J. Infrared Millimeter Waves **26**, 1661 (2005).
[2] R. Ulbricht, E. Hendry, J. Shan, T. F. Heinz, and M. Bonn, Rev. Mod. Phys. **83**, 543 (2011).
[3] T. Kampfrath, A. Sell, G. Klatt, A. Pashkin, S. Mährlein, T. Dekorsy, M. Wolf, M. Fiebig, A. Leitenstorfer, and R. Huber, Nat. Photonics **5**, 31 (2010).
[4] A. Pimenov, A. A. Mukhin, V. Y. Ivanov, V. D. Travkin, A. M. Balbashov, and A. Loidl, Nat. Phys. **2**, 97 (2006).

[5]A. Kirilyuk, A. V. Kimel, and Th. Rasing, Rev. Mod. Phys. **82**, 2731 (2010).
[6]R. Zhou, Z. Jin, G. Li, G. Ma, Z. Cheng, and X. Wang. Appl. Phys. Lett. **100**, 061102 (2012).
[7]K. P. Belov and V. I. Sokolov, Sov. Phys. Usp. **20**, 149 (1977).
[8]K. Kamazawa, D. Louca, R. Morinaga, T. J. Sato, Q. Huang, J. R. D. Copley, and Y. Qiu, Phys. Rev. B **78**, 064412 (2008).
[9]H. W. Capel, Physica **31**, 1152 (1965).
[10]M. Guilloti, A. Marchandt, V. Nekvasilt, and F. Tcheou, J. Phys. C: Solid State Phys. **18**, 3547 (1985).
[11]A. V. Inyushkin and A. N. Taldenkov, JETP **111**, 760 (2010).
[12]C. P. Slichter, *Principles of Magnetic Resonance* (Springer, New York, 1980).
[13]P. U. Jepsen, C. Winnewisser, M. Schall, V. Schyja, S. R. Keiding, and H. Helm, Phys. Rev. E **53**, 3052 (1996).
[14]Q. Wu and X.-C. Zhang, Appl. Phys. Lett. **67**, 3523 (1995).
[15]Z. Xu, J. Wen, T. Berlijn, P. M. Gehring, C. Stock, M. B. Stone, W. Ku, G. Gu, S. M. Shapiro, R. J. Birgeneau, and G. Xu, Phys. Rev. B **86**, 174419 (2012).
[16]H. Nojiri and Z. W. Ouyang, Terahertz Sci. Technol. **5**, 1 (2012).
[17]J. A. Koningstein and C. J. Kane-Maguire, Can. J. Chem. **52**, 3445 (1974).
[18]D. Boakes, G. Garton, D. Ryan, and W. P. Wolf, Proc. Phys. Soc. London A **76**, 663 (1959).
[19]G. R. Asatryan and V. A. Khramtsov, Tech. Phys. **55**, 74 (2010).
[20]J. Felsteiner and S. K. Misra, Phys. Rev. B **24**, 2627 (1981).
[21]E. Beaurepaire, J.-C. Merle, A. Daunois, and J.-Y. Bigot, Phys. Rev. Lett. **76**, 4250 (1996).
[22]E. Beaurepaire, G. M. Turner, S. M. Harrel, M. C. Beard, J.-Y. Bigot, and C. A. Schmuttenmaer, Appl. Phys. Lett. **84**, 3465 (2004).
[23]E. G. Villora, P. Molina, M. Nakamura, K. Shimamura, T. Hatanaka, A. Funaki, and K. Naoe, Appl. Phys. Lett. **99**, 011111 (2011).
[24]We note, however, that our recent study demonstrated that this assumption should be taken cautiously, as discussed in R. V. Mikhaylovskiy, E. Hendry, and V. V. Kruglyak, Phys. Rev. B **86**, 100405 (2012).
[25]V. V. Kruglyak, S. O. Demokritov, and D. Grundler, J. Phys. D: Appl. Phys. **43**, 264001 (2010).